PHYSICAL REVIEW B **96**, 121407(R) (2017)

Recognition of Fermi-arc states through the magnetoresistance quantum oscillations in Dirac semimetal Cd_3As_2 nanoplates

Guolin Zheng,[1] Min Wu,[1,2] Hongwei Zhang,[1,2] Weiwei Chu,[1,2] Wenshuai Gao,[1,2] Jianwei Lu,[1,2] Yuyan Han,[1] Jiyong Yang,[1] Haifeng Du,[1,3] Wei Ning,[1,*] Yuheng Zhang,[1] and Mingliang Tian[1,3,4,†]

[1]*Anhui Province Key Laboratory of Condensed Matter Physics at Extreme Conditions, High Magnetic Field Laboratory, Chinese Academy of Sciences, Hefei 230031, People's Republic of China*

[2]*Department of Physics, University of Science and Technology of China, Hefei 230026, People's Republic of China*

[3]*Department of Physics, School of Physics and Materials Science, Anhui University, Hefei 230601, Anhui, People's Republic of China*

[4]*Collaborative Innovation Center of Advanced Microstructures, Nanjing University, Nanjing 210093, People's Republic of China*

(Received 29 March 2017; published 27 September 2017)

Disjointed Fermi arcs in Weyl semimetals can intertwine with chiral bulk modes and participate in unusual closed magnetic orbits in the presence of a vertical magnetic field. Here, we carry out a quantum oscillation study of such unusual Weyl magnetic orbits in the Dirac semimetal Cd_3As_2, a close cousin of Weyl semimetals. We find that extra two-dimensional (2D) quantum oscillations emerge at high fields, which superimpose on a three-dimensional bulk background and can be attributed to the Weyl magnetic orbits, when the thickness of the nanoplates is smaller than the mean free path of the electrons. Further evidence of 2D quantum oscillations from the Weyl magnetic orbits is provided by nonlocal detection, which demonstrates an alternative way to study the quantum transport properties of Fermi arcs under magnetic fields.

DOI: 10.1103/PhysRevB.96.121407

Weyl semimetals (WSMs) are newly emergent topological states of matter whose low-energy bulk excitations can be described by the Weyl equations [1]. These low-energy quasiparticles behave as "Weyl fermions," well known in high-energy physics, and exhibit an apparent violation of charge conservation, leading to many exotic transport phenomena, such as chiral anomaly [2–8] and an anomalous Hall effect [9–12]. Another signature of the nontrivial topological nature of WSMs is the Fermi-arc surface state, which connects pairs of Weyl nodes with opposite chiralities [13–20]. Disjointed Fermi arcs can in principle be detected via quantum oscillatory experiments, if the electrons keep their phase coherence after periodic motion along the Weyl magnetic orbits traversing the bulk to connect the Fermi arcs on opposite surfaces [21]. Generally, quantum oscillations from surface Fermi arcs are mixed with bulk states, leading to a beating pattern [22]. The surface state contribution can only be identified in a frequency domain. Spin-polarized Fermi arcs behave as helical edge states, supporting nonlocal detection which may extract the surface quantum oscillations from large bulk backgrounds and provide other transport signatures of Weyl magnetic orbits.

In this Rapid Communication, we carry out a quantum oscillation study of the Weyl magnetic orbits in the Dirac semimetal Cd_3As_2, a close cousin of WSMs. We find that our Cd_3As_2 nanoplates exhibit extra weak two-dimensional (2D) oscillations superimposed on three-dimensional (3D) bulk oscillations at high fields, when the thickness of the Cd_3As_2 nanoplates is smaller than the quantum mean free path of the electrons. The analysis of the oscillation frequency reveals that the 2D oscillations at high fields can be attributed to the Weyl magnetic orbits connecting the Fermi arcs from opposite surfaces. Further evidence for the 2D oscillations of Weyl magnetic orbits is provided by nonlocal detection, which demonstrates an alternative way to study the Fermi arcs in WSMs.

Cd_3As_2 nanoplates were grown by chemical vapor deposition (CVD) methods on silicon substrates, as discussed elsewhere [4,5]. To improve the quality of the Cd_3As_2 nanoplates, a quartz tube was cleaned by ultrapure Ar gas for five times and a background vacuum as low as 15 mTorr was obtained prior to growth. Cd_3As_2 nanoplates of lengths up to 50 μm can be obtained, as shown in Fig. 1(a). Cd_3As_2-based quantum devices were fabricated by standard electron-beam lithography (EBL), followed by an Au(100 nm)/Ti(10 nm) evaporation and lift-off process.

In the Dirac semimetal Cd_3As_2, two sets of Weyl points with opposite chiralities are superimposed along the k_z direction, protected by the extra crystallographic symmetry from mixing and annihilation [14]. Considering a single pair of bulk Weyl nodes with chiralities ± 1, the Fermi arcs from two opposite real-space surfaces can participate in a Weyl magnetic orbit under a vertical magnetic field [21], as illustrated in Fig. 1(b). Typically, the Shubnikov–de Haas (SdH) oscillations in these Cd_3As_2 nanoplates exhibit a single frequency in a low-field region but show an extra oscillatory frequency above 5 T, as we can see in Fig. 1(c). This can also be seen in a fast Fourier transformation (FFT), where two oscillatory frequencies with $F_1 = 17.3$ T and $F_2 = 47.6$ T can be easily identified in sample S1. Bulk crystal Cd_3As_2 usually presents single-frequency quantum oscillations due to the near-isotropic Fermi surface [23,24]. The extra oscillation frequency at high fields is probably due to quantum oscillation from the Fermi arcs. As aforementioned, a prerequisite for the observation of Fermi-arc oscillations is that the electrons should keep their phase coherence after periodic motion along the Weyl magnetic orbits. That is, Fermi-arc oscillations can only be observed in thin Cd_3As_2 nanoplates with a magnetic field normal to the surface. Rotating the field B from the out-of-plane to in-plane direction, the surface Fermi-arc signals will gradually disappear, due to the loss of phase coherence. The observed

*ningwei@hmfl.ac.cn
†tianml@hmfl.ac.cn

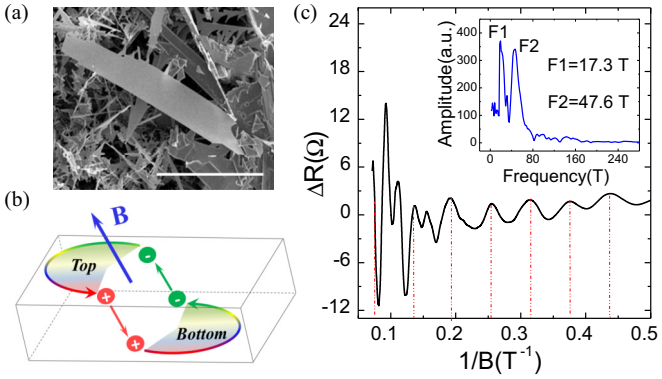

FIG. 1. (a) Scanning electron microscopy (SEM) image of the Cd_3As_2 nanoplates. Scale bar: 25 μm. (b) An illustration of the Weyl magnetic orbit in WSMs in the presence of a static magnetic field oriented perpendicular to the two opposite surfaces. (c) SdH oscillation components of longitudinal magnetoresistance in sample S1. Extra oscillations emerge at high fields. Inset: Corresponding FFT spectra of SdH oscillations.

Fermi-arc oscillations will only depend on the vertical field component, and thus lead to a 2D oscillation pattern. Such a 2D oscillation pattern in 3D Dirac semimetal Cd_3As_2 nanoplates is a transport signature of surface Fermi arcs, which can be confirmed by analyzing the angular-dependent quantum oscillations.

To confirm the 2D Fermi-arc oscillations, we now analyze the angle-dependent magnetoresistance in sample S2. Figure 2(a) shows the scanning electron microscopy (SEM) image of sample S2. For magnetic field B oriented perpendicular to the surface ($\theta = 0^\circ$), the longitudinal magnetoresistance ($R_{xx} = V_{54}/I_{12}$) of S2 shows apparent multiperiodic oscillations. While in the in-plane direction with B parallel to the current I ($\theta = 90^\circ$), single-frequency oscillations are revealed, as shown in Fig. 2(b). A plot of oscillatory components ΔR_{xx} vs $1/B$ under various tilted angles θ is presented in Fig. 2(c). Similar to sample S1, sample S2 shows single-frequency oscillations (bulk state) in a low-field region and the peak positions remain unchanged for various tilted angles θ, consistent with the near-isotropic band structure in Cd_3As_2. Above 8 T, extra oscillations appear sequentially and the oscillations from the bulk state seem to be overwhelmed near $\theta = 0^\circ$, as indicated by the blue arrow in Fig. 2(c). As θ increases, the newly emergent oscillations at high fields shrink and eventually vanish near $\theta = 90^\circ$. If we extract the perpendicular components of these quantum oscillations, both 3D (gray arrow) and 2D characters (gray lines) are revealed, as we can see in Fig. 2(d).

For further identification of the 2D Fermi-arc oscillations at high fields, we carry out extra measurements in sample S3, where the magnetic field is randomly rotated from the out-of-plane direction to the in-plane direction, as shown in Fig. 3. A similar situation has also been observed in sample S3, where extra oscillations emerge at high fields, as indicated by the blue arrow in Fig. 3(a). Those extra oscillations at high fields also exhibit a 2D character, as indicated by the gray lines in Fig. 3(b). As mentioned above, Fermi arcs can intertwine with the chiral bulk modes and participate in closed magnetic

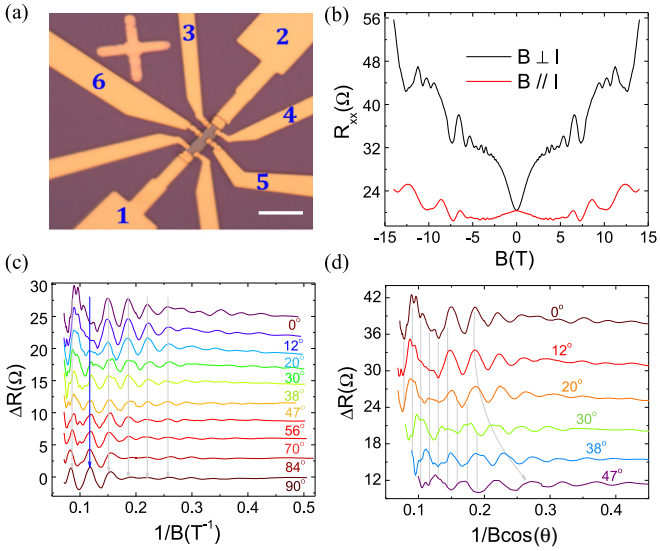

FIG. 2. (a) SEM image of sample S2. Scale bar: 10 μm. (b) The longitudinal magnetoresistance (MR) of sample S2 with B oriented perpendicular (black) and parallel (red) to the surface. (c) Detailed SdH oscillation components under different tilted angles θ, after subtracting the smooth background of the MR curves. Extra oscillations emerging at high fields have largely overwhelmed the bulk states near $\theta = 0^\circ$, as indicated by the blue arrow. (d) Angular dependence of the quantum oscillations. Both the 2D character (gray lines) for surface Fermi arcs and 3D (gray arrow) for bulk states are revealed. Note that some valleys of 2D surface oscillations are superimposed on the peaks of 3D bulk oscillations.

orbits, forming a 2D oscillation pattern. The observed extra 2D oscillations at high fields are most probably due to the Fermi-arc oscillations associated with unusual Weyl magnetic orbits. Now, we theoretically analyze the possibility of observing Fermi-arc states in these Cd_3As_2 nanoplates. According to a recent theory, the quantum oscillation frequency from the surface Fermi arcs can be estimated by the formula [21]

$$F_s = E_F k_0/(e\pi v_F), \tag{1}$$

where E_F is the Fermi level, k_0 is the arc length which is comparable with the separation of Dirac nodes ($\sim 0.1\,\text{Å}^{-1}$) [21,23], and v_F is the Fermi velocity. For simplicity and without loss of generality, we now calculate the Fermi energy and Fermi velocity in sample S3 via low-field quantum oscillations. According to the Lifshitz-Kosevich formula, the oscillation amplitudes can be written as [25]

$$\frac{\Delta\rho(T,B)}{\rho(B=0)} \propto \left(\frac{\hbar\omega_c}{E_F}\right)^{\frac{1}{2}} \frac{\alpha T m^*/B}{\sinh[\alpha T m^*/B]} \exp(-\alpha T_D m^*/B), \tag{2}$$

where T_D is the Dingle temperature, $\alpha = 2\pi^2 k_B/\hbar e$, and k_B is the Boltzmann constant. The cyclotron frequency is $\omega_c = eB/m^*$, with m^* the effective cyclotron mass. The Fermi energy E_F can be estimated by $E_F = m^* v_F^2$. Figure 3(c) shows the temperature dependence of the oscillation components ΔR_{xx} vs $1/B$ with the magnetic field oriented perpendicular to the surface ($\varphi = 0^\circ$). By fitting the oscillation amplitudes to the Lifshitz-Kosevich formula, we get the effective mass

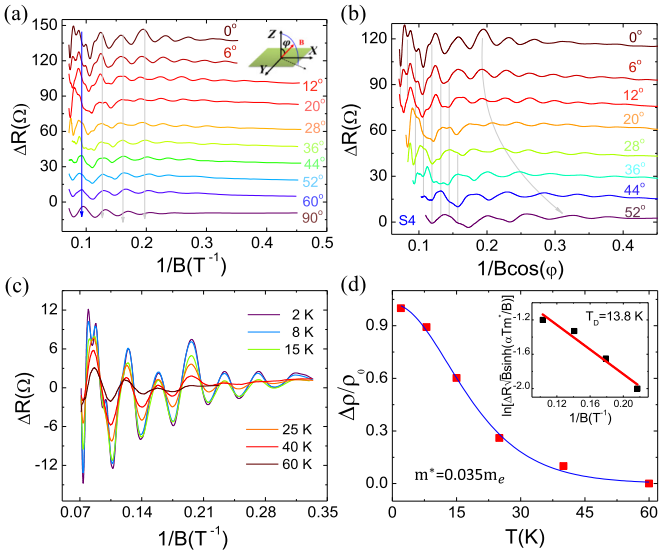

FIG. 3. (a) Angular-dependent MR oscillation components in sample S3 (∼80 nm) with B tilted randomly from the out-of-plane direction ($\varphi = 0°$) to in-plane direction ($\varphi = 90°$). Current is applied along the X direction. (b) SdH oscillation components vs $1/B\cos(\varphi)$ under different tilted angles φ. (c) Oscillation components as functions of $1/B$ for $\varphi = 0°$ under various temperatures. (d) Fitting the temperature-dependent oscillation amplitudes $\Delta\rho/\rho_0$ $(1/B = 0.242)$ generates an effective mass $m^* = 0.035m_e$. Inset: The fitted Dingle plot at 2 K generates a Dingle temperature $T_D = 13.8$ K.

$m^* = 0.035m_e$, as shown in Fig. 3(d). According to the Onsager relation, $F = (\hbar/2\pi e)S_F$, where F is the bulk oscillation frequency and S_F is the cross section of the Fermi surface, we can further calculate the Fermi wave vector k_F which is 0.031 Å^{-1}. Finally, the estimated Fermi energy is 210 meV, the Fermi velocity is 1.02×10^6 m/s, the calculated Fermi-arc oscillation frequency is $F_s \approx 66$ T. In our observation, the newly emergent oscillations at high fields have a spacing $\Delta(1/B) \approx 0.0132$ T^{-1}, generating an oscillation frequency of 75 T, which is quantitatively consistent with the theoretical calculation. To retain the phase coherence of the electrons after a periodic motion, the quantum mean free length l_Q should be larger than the thickness of the Cd_3As_2 nanoplates L. The quantum mean free path is given by $l_Q = v_F\tau_Q$, where the scattering time τ_Q is

$$\tau_Q = \hbar/(2\pi k_B T_D). \tag{3}$$

As shown in the inset of Fig. 3(d), the Dingle temperature T_D derived from the slope of the Dingle plot is 13.8 K. Thus, the calculated l_Q in sample S3 is about 90 nm, which is larger than the thickness of sample S3 (∼80 nm). Thus the Fermi-arc states, appearing as extra 2D oscillations in the high-field region, are confirmed by our experimental observations and previous discussions.

Figure 4 shows both local ($R_l = V_{54}/I_{12}$) and nonlocal ($R_{nl} = V_{56}/I_{43}$) magnetoresistance oscillation components of sample S2. Interestingly, the confirmed Fermi-arc oscillations in local detection can be significantly manifested in a nonlocal configuration, as indicated by the gray lines in Fig. 4(a)

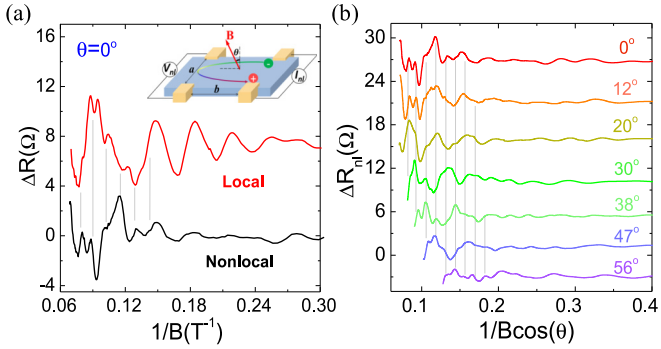

FIG. 4. (a) A comparison of the local ($R_l = V_{54}/I_{12}$) and nonlocal ($R_{nl} = V_{56}/I_{43}$) oscillation components in sample S2 for $\theta = 0°$. The 2D Fermi-arc oscillations in local detection can be significantly manifested in a nonlocal configuration with a vanishing bulk contribution. Inset: Schematic illustration of nonlocal detection. In sample S2, $b/a \sim 2.7$. (b) A nonlocal manifestation of the 2D Fermi-arc oscillations.

at $\theta = 0°$. Moreover, the bulk states, behaving as local magnetoresistance oscillations at low fields, have been largely suppressed here in the nonlocal configuration. Thus nonlocal detection may provide an effective way to extract Fermi-arc oscillations from large bulk backgrounds. If we track the nonlocal oscillations under different tilted angles θ, a more obvious 2D oscillation pattern can be obtained, as shown in Fig. 4(b). Bulk transport in a conventional metal, according to conventional diffusive electronics, satisfies Ohm's law and behaves as a local resistivity or conductive tensor [26]. However, in a nonlocal configuration, the bulk signal attenuates exponentially as an increase in the separation b [inset of Fig. 4(a)], according to the van der Pauw formalism [27]. In WSMs, the surface state as an open and disjointed Fermi arc provides a unique helical conductive path allowing for nonlocal detection, similar to the edge state in quantum spin Hall or quantum Hall systems [26]. However, different from the quantum spin Hall insulator state or a 3D topological insulator with gapped and insulating bulk states, the gapless bulk states in WSMs couple with surface Fermi arcs, leading to the quasiparticle scattering of surface Fermi arcs into the bulk [28]. The observed large nonlocal 2D Fermi-arc oscillations indicate that, in the presence of a vertical magnetic field, the surface quasiparticles driven by a Lorentz-like force can consecutively slide along the Fermi arcs and form conductive helical edge states, supporting nonlocal detection. We believe that the quasiparticle scattering of surface Fermi arcs into the bulk can be effectively suppressed by the magnetic field. The vanishing bulk signals demonstrate that nonlocality provides an alternative way to study the transport properties of Fermi-arc states in Dirac/Weyl semimetal systems.

Thus far, we have only considered a single pair of Weyl points with opposite chiralities. The Dirac semimetal Cd_3As_2 has two copies of superimposed Weyl points along the k_z direction, forming double Fermi-arc surface states [14]. Recently, Kargarian *et al.* [29] pointed out that in the presence of a surface perturbation, double Fermi arcs are unstable and can be continuously deformed into a closed Fermi contour. This surface perturbation can theoretically be introduced

by a magnetic field, which reduces the crystal symmetry [21,30]. The observed surface state oscillations in high fields may or may not originate from the unusual magnetic orbits, depending on the height of the Fermi level. In our Cd_3As_2 nanoplates, the Fermi level is about 200 meV above the Dirac point. The surface Fermi pockets might merge into the bulk state, forming a similar magnetic orbit, as discussed in Ref. [29]. Whereas there are no surface state oscillations in the low-field region in our samples, the initially observed 2D surface oscillations should be attributed to the magnetic orbits discussed in Ref. [21]. If Fermi arcs are deformed continuously by a magnetic field, a corresponding descent of the surface oscillation frequency should be observed. This seems not to be the case in our observations, because the surface oscillation frequency remains unchanged as field B increases. Extra nonlocal experiments are ongoing to investigate the deformation of Fermi-arc states under more intense magnetic fields.

We thank Professor E. V. Gorbar and Professor Kun Yang for fruitful discussions. This work was supported by the National Key Research and Development Program of China No. 2016YFA0401003 and No. 2017YFA0303201, and the Natural Science Foundation of China (Grants No. 11574320, No. 11374302, No. U1432251, and No. 11774353).

G.Z., M.W., and H.Z. contributed equally to this work.

[1] X. G. Wan, A. M. Turner, A. Vishwanath, and S. Y. Savrasov, Phys. Rev. B **83**, 205101 (2011).

[2] J. Xiong, S. K. Kushwaha, T. Liang, J. W. Krizan, M. Hirschberger, W. Wang, R. J. Cava, and N. P. Ong, Science **350**, 413 (2015).

[3] X. Huang, L. Zhao, Y. Long, P. Wang, D. Chen, Z. Yang, H. Liang, M. Xue, H. Weng, Z. Fang, X. Dai, and G. Chen, Phys. Rev. X **5**, 031023 (2015).

[4] C.-Z. Li, L.-X. Wang, H. Liu, J. Wang, Z.-M. Liao, and D.-P. Yu, Nat. Commun. **6**, 10137 (2015).

[5] H. Li, H. He, H.-Z. Lu, H. Zhang, H. Liu, R. Ma, Z. Fan, S.-Q. Shen, and J. Wang, Nat. Commun. **7**, 10301 (2015).

[6] Q. Li, Dmitri E. Kharzeev, C. Zhang, Y. Huang, I. Pletikosic, A. V. Fedorov, R. D. Zhong, J. A. Schneeloch, G. D. Gu, and T. Valla, Nat. Phys. **12**, 550 (2016).

[7] C.-L. Zhang, S.-Y. Xu, I. Belopolski, Z. Yuan, Z. Lin, B. Tong, G. Bian, N. Alidoust, C.-C. Lee, S.-M. Huang, T.-R. Chang, G. Chang, C.-H. Hsu, H.-T. Jeng, M. Neupane, D. S. Sanchez, H. Zheng, J. Wang, H. Lin, C. Zhang, H.-Z. Lu, S.-Q. Shen, T. Neupert, M. Z. Hasan, and S. Jia, Nat. Commun. **7**, 10735 (2016).

[8] G. L. Zheng, J. W. Lu, X. D. Zhu, W. Ning, Y. Y. Han, H. W. Zhang, J. L. Zhang, C. Y. Xi, J. Y. Yang, H. F. Du, K. Yang, Y. H. Zhang, and M. L. Tian, Phys. Rev. B **93**, 115414 (2016).

[9] A. A. Burkov and L. Balents, Phys. Rev. Lett. **107**, 127205 (2011).

[10] A. A. Burkov, M. D. Hook, and L. Balents, Phys. Rev. B **84**, 235126 (2011).

[11] G. Xu, H. Weng, Z. Wang, X. Dai, and Z. Fang, Phys. Rev. Lett. **107**, 186806 (2011).

[12] K.-Y. Yang, Y.-M. Lu, and Y. Ran, Phys. Rev. B **84**, 075129 (2011).

[13] Z. Wang, Y. Sun, X.-Q. Chen, C. Franchini, G. Xu, H. Weng, X. Dai, and Z. Fang, Phys. Rev. B **85**, 195320 (2012).

[14] Z. Wang, H. Weng, Q. Wu, X. Dai, and Z. Fang, Phys. Rev. B **88**, 125427 (2013).

[15] H. Weng, C. Fang, Z. Fang, B. A. Bernevig, and X. Dai, Phys. Rev. X **5**, 011029 (2015).

[16] S. M. Huang, S.-Y. Xu, I. Belopolski, C.-C. Lee, G. Q. Chang, B. K. Wang, N. Alidoust, G. Bian, M. Neupane, C. L. Zhang, S. Jia, A. Bansil, H. Lin, and M. Zahid Hasan, Nat. Commun. **6**, 7373 (2015).

[17] S. Y. Xu, C. Liu, S. K. Kushwaha, R. Sanker, J. W. Krizan, I. Belopolski, M. Neupane, G. Bian, N. Alidoust, T. R. Chang, H. T. Jeng, C. Y. Huang, W. F. Tsai, H. Lin, P. P. Shibayev, F. C. Chou, R. J. Cava, and M. Z. Hasan, Science **347**, 294 (2015).

[18] S. Y. Xu, I. Belopolski, N. Alidoust, M. Neupane, G. Bian, C. L. Zhang, R. Sankar, G. Q. Chang, Z. J. Yuan, C. C. Lee, S. M. Huang, H. Zheng, J. Ma, D. S. Sanchez, B. K. Wang, A. Bansil, F. C. Chou, P. P. Shibayev, H. Lin, S. Jia, and M. Z. Hasan, Science **349**, 613 (2015).

[19] B. Q. Lv, N. Xu, H. M. Weng, J. Z. Ma, P. Richard, X. C. Huang, L. X. Zhao, G. F. Chen, C. E. Matt, F. Bisti, V. N. Strocov, J. Mesot, Z. Fang, X. Dai, T. Qian, M. Shi, and H. Ding, Nat. Phys. **11**, 724 (2015).

[20] B. Q. Lv, H. M. Weng, B. B. Fu, X. P. Wang, H. Miao, J. Ma, P. Richard, X. C. Huang, L. X. Zhao, G. F. Chen, Z. Fang, X. Dai, T. Qian, and H. Ding, Phys. Rev. X **5**, 031013 (2015).

[21] A. C. Potter, I. Kimchi, and A. Vishwanath, Nat. Commun. **5**, 5161 (2014).

[22] P. J. W. Moll, N. L. Nair, T. Helm, A. C. Potter, I. Kimchi, A. Vishwanath, and J. G. Analytis, Nature (London) **535**, 266 (2016).

[23] T. Liang, Q. Gibson, M. N. Ali, M. H. Liu, R. J. Cava, and N. P. Ong, Nat. Mater. **14**, 280 (2015).

[24] S. Borisenko, Q. Gibson, D. Evtushinsky, V. Zabolotnyy, B. Büchner, and R. J. Cava, Phys. Rev. Lett. **113**, 027603 (2014).

[25] D. Shoenberg, *Mangetic Oscillations in Metals* (Cambridge University Press, Cambridge, UK, 1984).

[26] A. Roth, C. Brüne, H. Buhmann, L. W. Molenkamp, J. Maciejko, X.-L. Qi, and S.-C. Zhang, Science **325**, 294 (2009).

[27] L. J. van der Pauw, Philips Res. Rep. **13**, 1 (1958).

[28] E. V. Gorbar, V. A. Miransky, I. A. Shovkovy, and P. O. Sukhachov, Phys. Rev. B **93**, 235127 (2016).

[29] M. Kargarian, M. Randeria, and Y.-M. Lu, Proc. Natl. Acad. Sci. USA **113**, 8648 (2016).

[30] C. Zhang, A. Narayan, S. Lu, J. Zhang, X. Yuan, Y. Liu, J. Park, E. Zhang, W. Wang, S. Liu, L. Cheng, L. Pi, Z. Sheng, S. Sanvito, and F. Xiu, arXiv:1612.05873.